Magnetic Resonance in Medicine 56:432–438 (2006)

Rapid Cardiac-Output Measurement With Ungated Spiral Phase Contrast

Jong B. Park,[1*] Bob S. Hu,[1,2] Steven M. Conolly,[1,3] Krishna S. Nayak,[4] and Dwight G. Nishimura[1]

An ungated spiral phase-contrast (USPC) method was used to measure cardiac output (CO) rapidly and conveniently. The USPC method, which was originally designed for small peripheral vessels, was modified to assess CO by measuring flow in the ascending aorta (AA). The modified USPC used a 12-interleaf spiral trajectory to acquire full-image data every 283 ms with 2-mm spatial resolution. The total scan time was 5 s. For comparison, a triggered real-time (TRT) method was used to indirectly calculate CO by measuring left-ventricular (LV) volume. The USPC and TRT measurements from all normal volunteers agreed. In a patient with patent ductus arteriosus (PDA), high CO was measured with USPC, which agreed well with the invasive cardiac-catheterized measurement. In normal volunteers, CO dropped about 20–30% with Valsalva maneuvering, and increased about 100% after exercise. Continuous 28-s cycling between Valsalva maneuvering and free-breathing showed that USPC can temporally resolve physiological CO changes. Magn Reson Med 56:432–438, 2006. © 2006 Wiley-Liss, Inc.

Key words: cardiac output; phase contrast; quantification; fast imaging; flow; spiral

Cardiac output (CO), the total blood output from the left ventricle (LV) into the ascending aorta (AA), can be a key indicator for assessing patients with cardiovascular disease and can be an essential factor in monitoring the post-surgical or -medicated condition of patients (1). However, no gold standard exists for measuring CO. In current clinical settings, invasive methods using catheterization are generally used to measure CO, although they are not perfect. We propose here a novel noninvasive MRI approach to measure CO based on an ungated spiral phase-contrast (USPC) sequence. It was previously shown that USPC can rapidly, accurately, and reproducibly measure time-averaged flow rates in the femoral and renal arteries (2,3). However, measuring CO or flow in the AA using USPC presents different challenges compared to measuring flow in the small peripheral vessels. AA flow is faster and has even higher pulsatility and acceleration (4), and adjacent static material, which is helpful for correcting phase-offset errors in PC imaging (5), does not exist. In this study we show that modified USPC can rapidly and conveniently measure CO. For comparison we used a triggered real-time (TRT) imaging method (6,7) to indirectly calculate CO from an LV-volume measurement.

MATERIALS AND METHODS

Pulse Sequences

USPC (2,3) is a non-cardiac-synchronized PC technique (5) that uses interleaved spiral *k*-space trajectories (8). Figure 1 shows one example of the USPC pulse sequence, played out continuously with a short TR. The two flow encodings (FEs) in the through-plane direction are alternated every excitation, and the spiral readouts are rotated every odd excitation. In USPC, interleaved spiral trajectories (as opposed to Cartesian trajectories) provide significant flow-artifact suppression even with high spatial resolution, leading to accurate measurement of both velocity and vessel cross section (2). Moreover, by using a pseudo-randomized interleaf ordering (9) and a minimum-first-moment FE scheme ($M_1 = \pm \Delta M_1/2$) (5), flow artifacts can be further reduced (2).

For successful application of USPC to CO measurement, we carefully modified the original USPC method based on various in vivo and pulsatile-flow-phantom (Pump–1421, Harvard Apparatus, MA, USA) experiments. The resulting scan parameters of the modified USPC are summarized in Table 1. The modified USPC uses a 12-interleaf spiral trajectory to acquire full-image data every 283 ms with 2-mm spatial resolution. The rationales for the modifications are detailed in the Discussion section. The actual values of the scan parameters, such as maximum-velocity encoded (V_{enc}) and spatial resolution, were measured with the phantom scans before the in vivo experiments. We manually ordered the trajectories to have consecutive acquisitions maximally separated in *k*-space. If the spiral trajectories in *k*-space are numbered from 1 to 12 in terms of their consecutive rotation, the trajectories used in temporal order are as follows: {1, 7, 4, 10, 2, 6, 11, 3, 8, 12, 5, 9}. To achieve a spoiled-gradient-echo-type behavior, we used RF spoiling and a gradient spoiler on the slice-select gradient.

[1]Magnetic Resonance Systems Research Laboratory, Department of Electrical Engineering, Stanford University, Stanford, California, USA.

[2]Cardiovascular Medicine, Palo Alto Medical Foundation, Palo Alto, California, USA.

[3]Department of Bioengineering, University of California–Berkeley, Berkeley, California, USA.

[4]Electrical Engineering Department, University of Southern California–Los Angeles, Los Angeles, California, USA.

Grant sponsor: California Tobacco-Related Disease Research Program; Grant number: 9RT–0024; Grant sponsor: GE Healthcare.

*Correspondence to: Jong B. Park, Packard Electrical Engineering Building, Room 211, 350 Serra Mall, Stanford, CA 94305. E-mail: piquant@mrsrl.stanford.edu

Received 18 August 2005; revised 14 April 2006; accepted 25 April 2006.

DOI 10.1002/mrm.20970

Published online 26 June 2006 in Wiley InterScience (www.interscience.wiley.com).

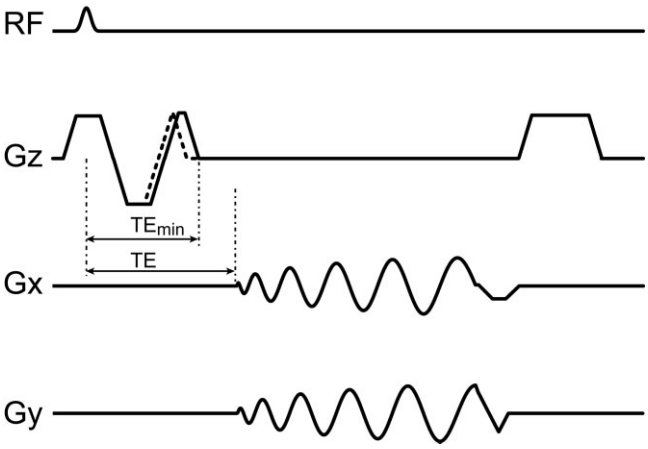

FIG. 1. USPC for CO measurement. The dashed line in the G_z-axis shows the alternate FE. A short Kaiser-windowed RF-pulse of 0.48 ms, a high gradient slew rate of 145 mT/m/ms, and the combination of the FE gradients with the slice-rephasing gradient enabled a TE_{min} of 2.2 ms for a 3-mm slice thickness and a 250-cm/s V_{enc}.

In the postprocessing stage of USPC, one must average over an integer multiple of cardiac cycles to acquire the appropriate time-average of periodic arterial flow. The proper integration interval can be extracted from a graph called a cumulative-average velocity plot (CAVP), which is constructed by using the same USPC raw-data sets for measuring CO (2). Each point of a CAVP is a velocity average acquired by using all the data collected up to that point in time. Figure 2 shows two examples of a CAVP that exhibit periodic-like behavior. Note that the CO measurement is acquired by averaging the data only from a certain interval, not necessarily including the data from the beginning of the scan, and thus the CO measurement may not be equal to the value in the cumulative plot. After the CAVP was constructed we chose the excitations that corresponded to the low-to-low dips of a CAVP covering an integer multiple of cardiac cycles. We then temporally averaged those selected excitations to produce two images with different FEs. Finally, we performed conventional PC postprocessing, i.e., we computed the phase difference and performed region-of-interest (ROI) segmentation on those two images to produce the CO measurement.

To reduce observer variability in segmenting ROIs for the CO measurement, we used a semiautomated process with thresholding (5) in a spatially interpolated magnitude image. First, a two-times-interpolated magnitude image was reconstructed with zero-padding (10). The interpolation reduces the influence of the position of the reconstruction grid without altering the accuracy of the flow quantification (11), and increases the number of pixels over the AA cross section, which can decrease inter- and intraobserver variability. Next, an approximate ROI was manually drawn around the AA in the color-scaled magnitude image. A color scale, rather than a gray scale, was used to help the observer draw the approximate ROI, and enhance the consistency among different data and different observers. Finally, we used a conventional thresholding technique that uses the peak magnitude pixel inside the lumen as a reference (5) to exclude unwanted pixels inside the ROI. We chose the threshold that produced the final ROI with a smooth circular vessel-boundary line. The inter- and intraobserver variability resulting from this ROI-segmentation scheme was measured with three observers.

TRT imaging provides high-temporal-resolution images and can automatically advance to a different slice position based on cardiac triggers (6,7). Using TRT with a fully-balanced steady-state free precession (SSFP) technique, one can measure LV volumes with multiple slices perpendicular to the long axis of LV within a single breath-hold of 10 R-R intervals (6). Hence, in a subject with no regurgitant flow at the valves, one can use TRT to indirectly calculate CO (L/min) by multiplying the stroke volume (L/beats) with the heart rate (beats/min), where the stroke volume is the difference between an end-diastolic volume and an end-systolic volume of LV. In our experiment, TRT used 20 interleaved spiral readouts and a TR of 5.9 ms to achieve an FOV of 20 cm and a spatial resolution of 1.8×1.8 mm^2. Other scan parameters for TRT were a flip angle of 60°, slice thickness of 10 mm, and no interslice gap.

Experimental Methods

We performed studies on a 1.5 T GE Signa CV/I whole-body scanner (GE Healthcare, Milwaukee, WI, USA) with gradients capable of 40 mT/m amplitude and 150 mT/m/ms slew rate, and a receiver capable of 4 μs sampling. We used a body coil for the RF transmission and a 5-inch-diameter surface coil for the signal reception. The surface coil was placed anteriorly with the subject in a supine position. Nine normal volunteers (six males and three females, age range = 24–40 years) and one patient (female, 28 years old) with patent ductus arteriosus (PDA) were scanned. Approval from the institutional review board and informed consent from the subjects were obtained before the scans were performed.

In three normal volunteers, we also measured abnormal (decreased or increased) CO that was intentionally induced by physiological maneuvers. The first subject un-

Table 1
USPC Scan Parameters for Measuring CO ($USPC_{CO}$) and the Original Scan Parameters for Measuring Peripheral-Artery Flow ($USPC_o$)

Index[a]	1	2	3	4	5	6	7	8	9	10
	N	TR	FOV	Δx	Δz	θ	TE (TE_{min})	Slice	V_{enc}	T_{read}
$USPC_{CO}$	12	11.8 ms	24 cm	2 mm	3 mm	10°	3.0 (2.2) ms	Axial	250 cm/s	4.8 ms
$USPC_o$	40	15 ms	30 cm	1 mm	10 mm	30°	3.5 (3.5) ms	Oblique	100 cm/s	7.4 ms

[a]1 = number of interleaved spiral trajectories, 2 = pulse repetition time, 3 = field of view, 4 = spatial resolution, 5 = slice thickness, 6 = flip angle, 7 = TE_{min} = minimum-possible-TE defined in Fig. 1, 8 = imaging-slice orientation, 9 = maximum-velocity encoded, 10 = readout time.

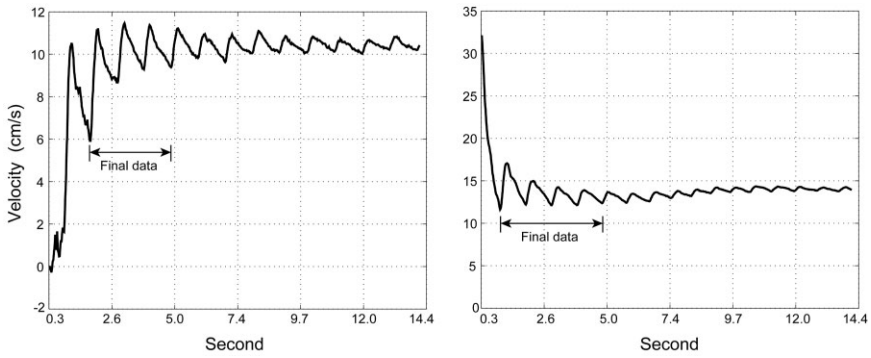

FIG. 2. Examples of a CAVP constructed from the same USPC raw-data sets for CO measurement in two normal subjects. To show that a CAVP eventually approaches the time-averaged velocity of interest, the scan time was extended to 14 s. The arrows show possible intervals for the final data set covering an integer multiple of cardiac cycles.

derwent Valsalva maneuvering (1) to decrease CO. On the second subject we performed a continuous 28-s Valsalva on-off experiment to show that USPC can temporally resolve physiological changes. In this experiment the subject continuously alternated between Valsalva maneuvering and free-breathing, while being scanned with USPC. Finally, the third subject performed a 5-min running exercise after the normal CO was measured, and the postexercise CO changes were continuously measured with USPC for 4 min.

The study protocol was as follows: First, TRT measured LV volumes using an interactive real-time imaging system (9). All measurements were done with a breath-hold at a neutral respiratory position except for the cases in which Valsalva maneuvering was performed. The scan time for each measurement with TRT was 9–15 s, depending on the heart rate (6). Next, we repositioned the coil and the subject for USPC scans using the same interactive real-time system to orient the AA perpendicular to the axial imaging plane at isocenter. Note that the small amount (<5–10%) of blood flow into the coronary artery (1) is neglected by placing the imaging slice as described above. CO with free-breathing was also measured with USPC in all normal subjects. As an additional reference measurement, the cardiac-catheterized Fick method was used in the PDA patient. The scan time for USPC was 5 s for each measurement except for the continuous Valsalva on-off and postexercise scans.

RESULTS

Figure 3a shows the CO measurements obtained. The error bars for each measurement represent the standard deviations (SDs) of repeated measurements for each subject in a single session. Figure 3b and c show the differences between USPC with breath-holding and TRT, and USPC with

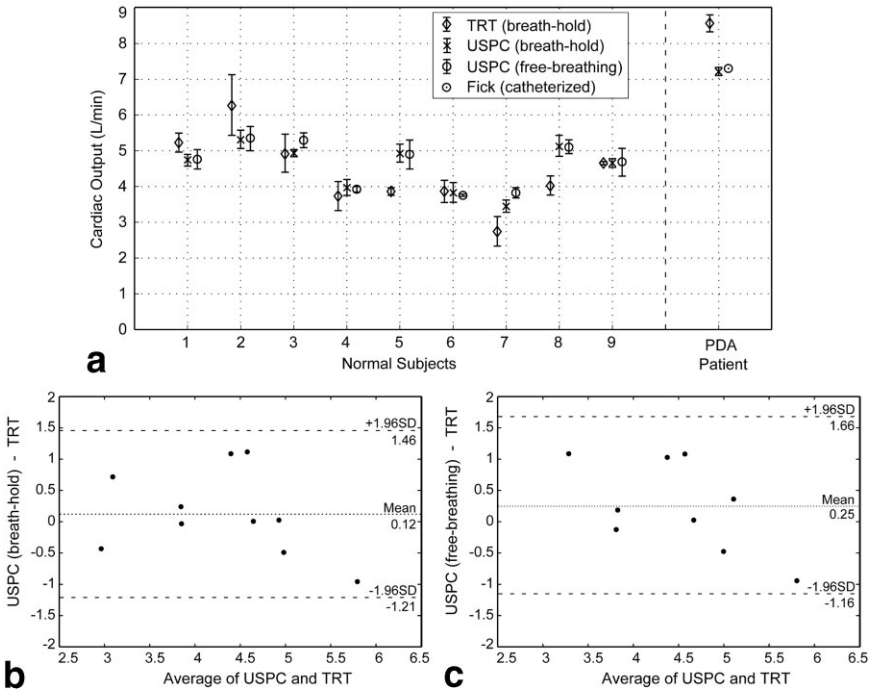

FIG. 3. CO measurements. **a:** USPC and TRT measured CO obtained in each subject three and two times, respectively. For the patient with PDA, the catheterized method was also used as a reference. **b** and **c:** Differences in the mean values of USPC and TRT measurements for normal subjects are plotted against their average. The Valsalva-maneuvering result shown in Fig. 5a is also included in **b**.

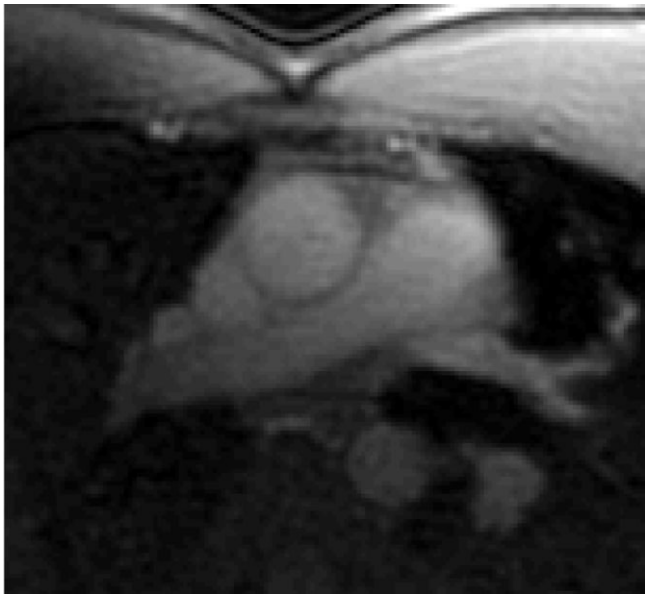

FIG. 4. Example of a USPC magnitude image with twofold interpolation.

free-breathing and TRT, respectively, in a Bland-Altman plot (12). In all normal subjects, USPC with breath-holding and TRT measurements agreed, as shown in Fig. 3b. USPC measurements with free-breathing showed slight overestimation (Fig. 3c) compared to those with breath-holding. In the PDA patient, USPC with breath-holding measured high abnormal CO, which agreed well with the Fick measurement (Fig. 3a). (The USPC measurement with free-breathing could not be collected on this patient due to early termination of the study.) Figure 4 shows a USPC magnitude image exhibiting minimal flow artifacts.

As expected, CO dropped about 20–30% with Valsalva-maneuvered breath-holding compared to normal breath-holding (Fig. 5a). The continuous 28-s Valsalva on-off experiment showed that USPC can temporally resolve physiological changes (Fig. 5b). Moreover, CO increased about 100% after the exercise, as expected, and gradually decreased while the subject rested inside the scanner (Fig. 6). Even with the extensive chest movement from breathing during the resting period, only a slight increase of measurement fluctuation was seen.

Three observers independently segmented ROIs on the data sets for normal subjects, each consisting of three CO-measurement data per subject. Figure 7 shows that the interobserver variability (<10%) was similar to the intraobserver variability, which suggests that measurement variability is not likely to increase with different observers.

DISCUSSION

The results show that normal and abnormal (high or low) CO can be rapidly, accurately, and consistently measured using USPC. However, in subjects 5 and 8, the normal CO measured with USPC was about 20% higher than the CO calculated with TRT (Fig. 3). Although the exact cause of this discrepancy is unknown, note that only subjects 5, 7, and 8 underwent Valsalva in addition to normal breath-holding. (Valsalva data for subject 7 are not shown, because the results are similar to those in Fig. 5.) Further investigation is needed to explain this discrepancy with respect to the complicated study protocol involving physiological maneuvering. Note that for most clinical applications, the precision and reproducibility in CO measurement are more important than the absolute accuracy.

The scan time of USPC depends on how many cardiac cycles are used to measure the appropriate time-average. Partial-averaging errors occur in the postprocessing stage when the number of excitation sets selected to reconstruct the final temporally-averaged image does not equal an integer multiple of N (2). With typical flow waveforms of AA, data over at least three to four cardiac cycles should be temporally averaged to lower partial-averaging errors down to <5%, which can be shown by simulations. Thus, we chose a 5-s scan time to produce CAVPs showing more than three to four cardiac cycles (Fig. 2). One can choose longer scan times to minimize the SD, as can be inferred from the fact that a CAVP eventually approaches the time-average of interest. However, a scan time of 14 s does not show noticeable improvement (Fig. 8). This is most likely due to the fact that in four cardiac cycles at 60 beats per minute, *k*-space data are already averaged 14 or 15 times. Note that one can use scan times shorter than 5 s, but the measurement error may increase.

The rationales for the modified USPC scan parameters in Table 1 are as follows: It is possible to achieve higher spatial resolution (<2 mm) and a larger FOV (>24 cm)

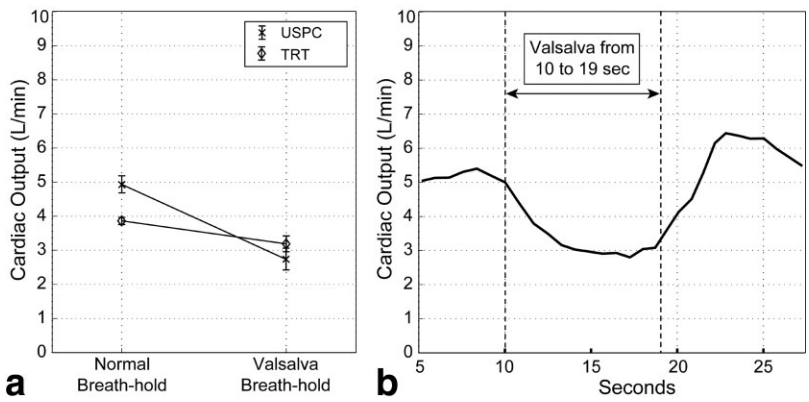

FIG. 5. Valsalva-maneuvering results. **a:** USPC-measured Valsalva-maneuvered CO of subject 5 in Fig. 3. **b:** CO changes measured by USPC corresponded well with the Valsalva maneuvering performed by subject 8 in Fig. 3.

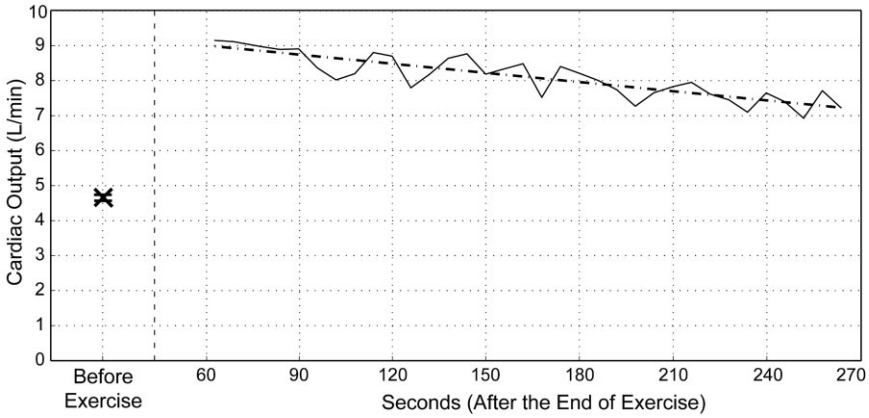

FIG. 6. Stress-study results. USPC measured CO of subject 9 in Fig. 3 before and after the 5-min running exercise. The straight dashed line is fitted over the CO measurements in a least-squares sense. Note the different scale of the horizontal axis compared to Fig. 5b.

with USPC (2). However, we used a smaller imaging-matrix size to reduce the total scan time for one complete image ($N \cdot$ TR) because a short $N \cdot$ TR can also reduce flow artifacts, which are likely to increase in AA compared to peripheral vessels. The higher peak velocity in AA can cause overestimation due to more pronounced in-flow enhancement of fast-moving spins, i.e., the higher signal contribution from in-flowing spins (2,13). In-flow enhancement can cause overestimation when the signals are complex-averaged (13). With USPC this complex averaging happens during the temporal averaging process before PC processing. However, a lower flip angle decreases the in-flow enhancement (13), and a thinner slice further decreases the RF saturation of slow-moving spins. From flow-phantom and in vivo experiments with a slice thickness of 1–10 mm and flip angles of 5–45°, we found that a 3-mm slice and 10° flip angle produced the most accurate flow measurement. We compensated for the loss of SNR due to the thin slice and low flip angle by temporally averaging the data over more than 3 s. The short minimum-possible TE (TE_{min}) significantly reduced the second-order gradient moment before the readout, and thus minimized phase errors caused by high acceleration. A less sharp slice profile caused by a short RF pulse had a minimal effect on the through-plane-flow quantification since the slice was thin relative to the size and curvature of typical AAs. A relatively large V_{enc} reduces the error caused by in-flow enhancement and by asymmetry of the velocity distribution in a voxel (2,16,17). However, if V_{enc} is large, the measurement becomes more sensitive to phase errors because smaller phase shifts are induced by flow (5). Thus,

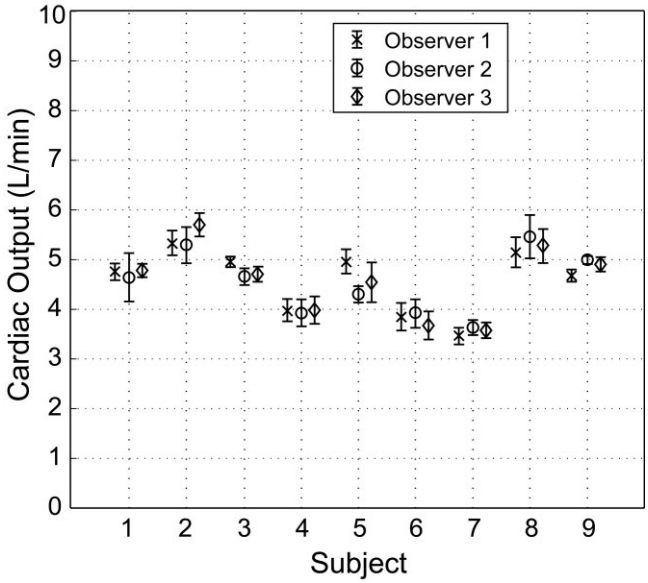

FIG. 7. Inter- and intraobserver variability in segmenting ROIs for CO measurement. Three observers independently segmented the ROIs on normal subject data.

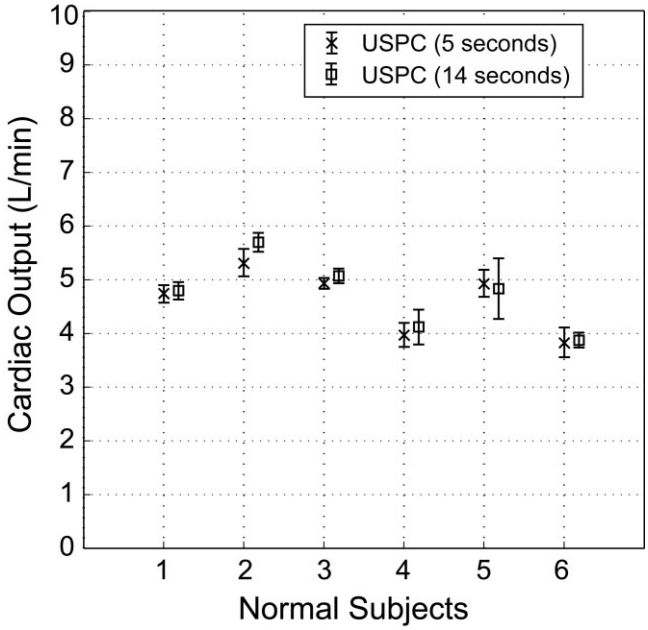

FIG. 8. Comparison of 5-s and 14-s USPC scan times. The 14-s scans were also performed on the first six subjects in Fig. 3, and the measurements were obtained by temporally averaging more than 10 cardiac cycles from the 14-s CAVPs.

we performed in vivo and flow-phantom experiments using V_{enc}'s of 150–500 cm/s, and found that 250 cm/s provided an adequate balance between the reduced asymmetry and in-flow errors and the reduced phase errors.

In PC imaging, if the eddy-current-induced phase offset is corrected by extrapolating (rather than interpolating) a linear phase fit from static material not surrounding the vessel, a large error can result when slight inaccuracy exists in the first-order term of the fit. This is the case for CO measurement (Fig. 4). Scans of a large ball phantom with our specific scanner showed that the physical Z-gradient caused the least eddy-current-induced fields, and especially minimized the first-order term of the phase offsets. Thus, although oblique slices can be used with USPC, we used an axial slice, i.e., the FEs were only on the physical Z-gradient. This was to minimize the eddy-current-induced phase offset in the first place rather than to postcorrect the offset. Note that we were always able to find the slice location in which the axial slice was relatively perpendicular to AA. The use of a thin slice and relatively short TE also minimized possible errors from oblique vessel orientation (5). Moreover, the use of an axial slice also reduced phase errors from the unequal concomitant fields of the two FE gradients because the lowest-order concomitant-field equation reduced to a single term, which is four times smaller than other terms (14). By placing the imaging region at isocenter, we further reduced the concomitant phase errors (14) and also reduced any image blurring that may result from the concomitant fields of spiral readout gradients (15).

In most spiral PC methods for quantifying through-plane flow, TE is usually set equal to TE_{min} in order to minimize TR (2,7). However, if TE equals TE_{min}, then the start of the readout gradients, corresponding to the *k*-space-origin, overlaps in time with the eddy-current-induced fields. This overlap distorts data near the *k*-space origin, and thus the amplitude and linear variation of the induced phase offsets across the image are likely to be increased. To prevent this overlap, we used a TE slightly longer than TE_{min}. From phantom scans using increments of 0–2 ms, only a small increment (0.8 ms) was needed with our USPC implementation. Phantom scans also showed that the combined use of this dead-time and the isocentered axial slice reduced the eddy-current-induced phase errors to a level that obviated the need for any postcorrection. Note that considering the scan parameters and the characteristics of AA, a TE of 3 ms was sufficiently short to prevent the displacement of the fast moving spins from causing measurement errors.

An alternative to USPC is real-time spiral PC imaging (7). Both of these methods involve ungated acquisitions with a short TR; however, USPC uses more interleaves to achieve higher spatial resolution for reducing partial-volume averaging (5). For example, two- and 12-shot spiral trajectories achieve an approximately 6.5- and 2-mm spatial resolution, respectively, assuming the same FOV and TR. The cost of improved spatial resolution is a longer $N \cdot$ TR, which can lead to motion artifacts. Spiral trajectories, however, help reduce these artifacts compared to Cartesian trajectories (2,3). A longer acquisition window may lead to flow measurement errors from temporal averaging, an effect similar to partial-volume averaging. In general, a measurement error can occur when a pixel contains a distribution of velocities that is asymmetric about the desired mean velocity (velocity-dependent in-flow enhancement exacerbates this error) (5,16,17). With partial-volume averaging, a velocity distribution exists because of different velocities present in a relatively large pixel (5). Similarly with temporal averaging, a velocity distribution effectively exists in a pixel if velocity changes occur (typically from through-plane flow) occur over the course of the long acquisition window. In our implementation of USPC, a relatively thin slice, low flip angle, and large V_{enc} reduced the errors from this temporal-averaging effect.

In-plane vessel motion, which can change the velocity seen by a particular pixel, is another issue of concern because of the long acquisition window. However, the effect of such motion can be modeled as the temporal-averaging effect as well, and is thus reduced by our implementation. Moreover, the localizing scans in all subjects showed that the position and diameter of AA changed by only a few pixels. The minimal effect of vessel motion is further illustrated by the close agreement between the breath-holding and free-breathing results. However, if the intraluminal signal overlaps the empty pixels near the AA during the scan because of increased AA movement, flow rates are overestimated in those pixels (5,16,17), similar to partial-volume averaging with empty surrounding pixels. The slight overestimation of the free-breathing results from subjects 3 and 7 is likely the result of increased AA movement.

A real-time PC technique can temporally resolve AA flow changes within a cardiac cycle (7,18,19). In a study using a single-shot EPI *k*-space trajectory, a recent real-time PC method showed the potential to measure CO in pediatric patients (19), and agreement with a cardiac-synchronized PC method was seen. However, although a short TR (19.4 ms) and scan time (9.5 s) were used, an overestimation was observed. Using the analyses in this paper, one can show that the overestimation is likely caused by relatively low in-plane spatial resolution (2.7 mm), thick slice (8 mm), high flip angle (40°), and low V_{enc} (200 cm/s). A cardiac-synchronized PC technique can also temporally resolve AA flow changes within a cardiac cycle, and thus can measure CO (20). However, this technique is more prone to errors from irregular heartbeats and the requirement of longer breath-holds.

CONCLUSIONS

This paper shows that in vivo CO can be rapidly, accurately, and consistently measured without cardiac synchronization by using USPC. In addition to normal CO, high abnormal CO in a PDA patient was also accurately and consistently measured with USPC. Changes of CO in normal subjects with physiological maneuvering were also clearly shown with USPC. Finally, the short scan time of USPC enabled the continuous monitoring of CO changes. As suggested by the result from continuous USPC scanning, the sensitivity and high temporal resolution of USPC to physiological CO changes may provide insights into the pathophysiology and response to therapy for a diverse set of patients. Using USPC in combination with an LV-volume measurement, the regurgitant volume may be quantified in patients with aortic valvular disease.

REFERENCES

1. Braunwald E. Heart disease: a textbook of cardiovascular medicine. Philadelphia: Saunders; 1980. 1943 p.
2. Park JB, Olcott EW, Nishimura DG. Rapid measurement of time-averaged blood flow using ungated spiral phase-contrast. Magn Reson Med 2003;49:322–328.
3. Park JB, Santos JM, Hargreaves BA, Nayak KS, Sommer G, Hu BS, Nishimura DG. Rapid measurement of renal artery blood flow with ungated spiral phase-contrast MRI. J Magn Reson Imaging 2005;21:590–595.
4. Strandness DE. Duplex scanning in vascular disorders. New York: Raven Press; 1993. xii, 329 p.
5. Pelc NJ, Sommer FG, Li KC, Brosnan TJ, Herfkens RJ, Enzmann DR. Quantitative magnetic resonance flow imaging. Magn Reson Q 1994;10:125–147.
6. Narayan G, Nayak K, Pauly J, Hu B. Single-breathhold, four-dimensional, quantitative assessment of LV and RV function using triggered, real-time, steady-state free precession MRI in heart failure patients. J Magn Reson Imaging 2005;22:59–66.
7. Nayak KS, Hu BS. Triggered real-time MRI and cardiac applications. Magn Reson Med 2003;49:188–192.
8. Ahn CB, Kim JH, Cho ZH. High-speed spiral-scan echo planar NMR imaging—I. IEEE Trans Med Imaging 1986;MI-5:2–7.
9. Kerr AB, Pauly JM, Hu BS, Li KC, Hardy CJ, Meyer CH, Macovski A, Nishimura DG. Real-time interactive MRI on a conventional scanner. Magn Reson Med 1997;38:355–367.
10. Parker DL, Du YP, Davis WL. The voxel sensitivity function in Fourier transform imaging: applications to magnetic resonance angiography. Magn Reson Med 1995;33:156–162.
11. Hoogeveen RM, Bakker CJ, Viergever MA. MR phase-contrast flow measurement with limited spatial resolution in small vessels: value of model-based image analysis. Magn Reson Med 1999;41:520–528.
12. Bland JM, Altman DG. Statistical methods for assessing agreement between two methods of clinical measurement. Lancet 1986;1:307–310.
13. Polzin JA, Alley MT, Korosec FR, Grist TM, Wang Y, Mistretta CA. A complex-difference phase-contrast technique for measurement of volume flow rates. J Magn Reson Imaging 1995;5:129–137.
14. Bernstein MA, Zhou XJ, Polzin JA, King KF, Ganin A, Pelc NJ, Glover GH. Concomitant gradient terms in phase contrast MR: analysis and correction. Magn Reson Med 1998;39:300–308.
15. King KF, Ganin A, Zhou XJ, Bernstein MA. Concomitant gradient field effects in spiral scans. Magn Reson Med 1999;41:103–112.
16. Hamilton CA, Moran PR, Santago 2nd P, Rajala SA. Effects of intravoxel velocity distributions on the accuracy of the phase-mapping method in phase-contrast MR angiography. J Magn Reson Imaging 1994;4:752–755.
17. Wolf RL, Ehman RL, Riederer SJ, Rossman PJ. Analysis of systematic and random error in MR volumetric flow measurements. Magn Reson Med 1993;30:82–91.
18. van den Hout RJ, Lamb HJ, van den Aardweg JG, Schot R, Steendijk P, van der Wall EE, Bax JJ, de Roos A. Real-time MR imaging of aortic flow: influence of breathing on left ventricular stroke volume in chronic obstructive pulmonary disease. Radiology 2003;229:513–519.
19. Korperich H, Gieseke J, Barth P, Hoogeveen R, Esdorn H, Peterschroder A, Meyer H, Beerbaum P. Flow volume and shunt quantification in pediatric congenital heart disease by real-time magnetic resonance velocity mapping: a validation study. Circulation 2004;109:1987–1993.
20. Chatzimavroudis GP, Zhang H, Halliburton SS, Moore JR, Simonetti OP, Schvartzman PR, Stillman AE, White RD. Clinical blood flow quantification with segmented k-space magnetic resonance phase velocity mapping. J Magn Reson Imaging 2003;17:65–71.